J. Fluid Mech. (2003), *vol.* 496, *pp.* 33–62.
DOI: 10.1017/S0022112003006517 Printed in the United Kingdom

Patterns of solidification in channel flows with surface cooling

By ROSS W. GRIFFITHS[1], ROSS C. KERR[1] AND KATHARINE V. CASHMAN[2]

[1]Research School of Earth Sciences, Australian National University, Canberra, ACT 0200, Australia
[2]Department of Geological Sciences, University of Oregon, Eugene, OR 97403-1272, USA

(Received 6 March 2003)

Understanding the rates of cooling and solidification in laminar flows down sloping channels is central to predicting the advance of lava flows. The mechanisms involved include thermal convection and a competition between shear strain rate and the rate of formation of solid at the chilled surface of the flow. We report experiments in which polyethylene glycol wax flows in a laminar fashion down an inclined, open channel of rectangular cross-section under cold water. Two distinctly different flow regimes are recognized: 'tube' flow in which solidification of the flow surface creates a stationary roof while melt continues to flow through a relatively well-insulated 'tube' beneath, and a 'mobile crust' regime in which a solid surface crust develops only in the centre of the channel. In the latter regime the crust is carried down the channel, separated from the walls by crust-free shear regions in which cooling produces only dispersed fragments of solid owing to the effects of shearing. This flow structure is quasi-invariant over a large distance downstream. We show that thermal convection takes place in organized rolls that have axes aligned with the shear flow, and conclude that transition between the two flow regimes occurs at a critical value of the combined parameter $\vartheta = \psi(Ra/R_0)^{1/3}$, where $\psi = U_0 t_s/H_0$ is the ratio of a surface solidification timescale t_s to a shearing timescale H_0/U_0, H_0 and U_0 are the flow depth and centreline surface velocity in the absence of solidification, Ra is a Rayleigh number and R_0 is a constant.

1. Introduction

The flow and solidification of molten materials are intimately coupled, with flow influencing cooling and the consequent solidification in turn modifying the flow. For free-surface flows heat loss is commonly greatest at the surface, where solidification can form a crust that inhibits continued spreading, as well as insulating the flow against further cooling (Fink & Griffiths 1990, 1992; Kilburn 1993). In this paper we are concerned with the occurrence and distribution of solidification due to heat loss from a free surface during laminar gravity-driven flow down a slope.

In a particularly dramatic class of flows involving cooling and solidification, molten basaltic lava from large volcanic eruptions is often channelled into rapidly flowing rivers of melt (figure 1). On Hawai'i the channels are commonly 10–100 m wide and of the order of 10 km in length, with flow 2–10 m deep during its active period (Lipman & Banks 1987; Cashman, Pinkerton & Stephenson 1998). Much longer channels, up to 750 km in length, were important in transporting lavas from large prehistoric flood basalt eruptions (Shaw & Swanson 1970; Tolan *et al.* 1989). The rate of advance and

FIGURE 1. Photograph of braided lava channels during eruption of Pu'u 'O'o, Kilauea Volcano, Hawai'i (Episode 5, 1983). Photograph courtesy of the United States Geological Survey.

final length of these flows are expected (at least in some cases) to be strongly influenced by cooling and solidification (Walker 1973; Crisp & Baloga 1994; Pinkerton & Wilson 1994; Cashman *et al.* 1998). Indeed, the cooling will depend on the manner in which solidification occurs. Similar issues may arise in industrial processes involving melts, where, for example, the clogging of channels or the formation of surface textures may result from solidification during flow. In this paper we address solidification in the case of flow down a simple inclined channel and explore the ways in which solid surface crust forms in the presence of shear. The results are a starting point towards a better understanding of the effects of solidification on the rates of flow cooling and advance, but these consequences are not examined here.

Subaerial lava flows cool primarily by radiative heat loss from incandescent lava, while those under water are cooled by convection or boiling of the water (Wilson & Head 1983; Griffiths & Fink 1992*a*, *b*; Griffiths 2000). Many basaltic lava channels feature surface rafts of cooled and solidified melt (which appears dark due to its lower radiative temperature; figure 1). The solid shows varying extents of fragmentation and dispersal, but the surface remains largely mobile and the solid is carried along by the flow. Also common are lava tubes, which are channels that become fully encased by a roof of solidified lava (Peterson *et al.* 1994). Tubes can arise when enough solid develops on the flow surface to form a connected roof over the flow. The rigid roof greatly reduces the rate of heat loss (Kauahikaua *et al.* 1998) and hence enables the lava to flow much greater distances than would be possible if the roof were continuously disrupted (Cashman, Thornber & Kauahikaua 1999; Keszthelyi 1995; Kerr 2001). Thus a fundamental question in volcanology is the relationship between stable crust formation and flow conditions. Understanding controls on crustal stability is central to both estimates of the rates and volumes of prehistoric eruptions (e.g. Shaw & Swanson 1970; Walker 1973) and predictions of advance rates and flow

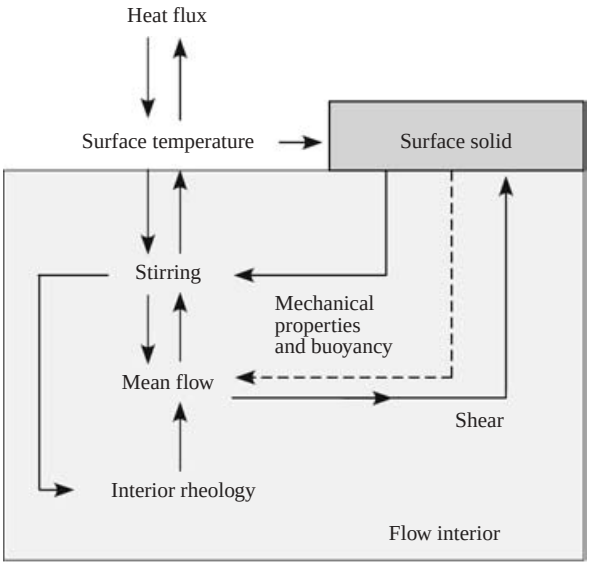

FIGURE 2. Schematic diagram of interactions that cause solidification to affect channel flows and their rates of cooling. For example, surface solid influences surface temperature, not directly, but through its mechanical influence on internal stirring.

paths of future eruptions. Similar questions arise in attempting to infer the geological histories of Venus, Mars and the Moon from remote images of morphological features on their surfaces (Hulme 1974; Mouginis-Mark, Wilson & Zuber 1992; Baker *et al.* 1997; Sakimoto, Crisp & Baloga 1997; Zimbelman & Gregg 2000).

We focus here on the processes that govern the flow through an existing channel. One difficulty encountered is that the formation of even thin solid on the surface might influence the rate of cooling of the flow (Crisp & Baloga 1990, 1994), while larger amounts of solid can also modify the velocity distribution (figure 2). The effect of solidification on cooling is a result of the greater mechanical stability of the solidified material. The mechanical stability tends to reduce stirring, divergence of surface velocities and exposure of fresh hot melt to the surface, relative to a purely molten flow. In order to predict flow cooling it is necessary to predict the distribution and mechanical effects of surface solid, and in particular, whether there will be areas of exposed melt or a fixed insulating roof. Some progress has been made in estimating the rate of heat loss from channel flows by empirical parameterization of the fraction of observed flow surfaces that exposes incandescent melt (Crisp & Baloga 1990). This parameterization has been incorporated into a simple numerical stream-tube model (Harris & Rowland 2001), which also attempts to account for stirring of a cooled surface layer into the underlying core of the flow as a result of gravitational instability, turbulence or channel irregularity. However, while parameterized modelling can explain the rate of flow front advance and final length of specific individual flows, successful extrapolation to new cases requires an understanding of the processes at work and formulation of a parameterization scheme based on underlying physical principles.

Progress in understanding the interactions of flow and solidification has been made using laboratory experiments with polyethylene glycol (PEG) wax, a clear, water-soluble fluid having a freezing temperature conveniently close to room temperature

(Hallworth, Huppert & Sparks 1987; Fink & Griffiths 1990, 1992; Griffiths & Fink 1993; Gregg & Fink 2000). In these experiments, molten wax was released from a small vent beneath cold water to form a viscous gravity current. High-Rayleigh-number convection in the water carried heat away from the flow surface (replacing predominantly radiative cooling of subaerial lavas). These slow wax flows on a sloping plane extended down-slope, either in an open channel constructed by the formation of lateral levees of solidified wax, or in internal channels insulated by a rigid roof. The style of flow depended primarily on the bottom slope and the dimensionless parameter

$$\psi = U_0 t_s / H_0, \tag{1}$$

where t_s is a timescale for cooling of the flow surface temperature down to the solidification temperature (in the presence of turbulent convection in the overlying water but conduction alone in the wax), and U_0 and H_0 are velocity and depth scales for viscous gravitational spreading of an isothermal fluid (which can be expressed in terms of the source volume flux, gravity and viscosity). The parameter ψ is simply a measure of the rate of solidification relative to the rate of flow expected without solidification (Griffiths & Fink 1993; Griffiths 2000). These studies revealed a number of regimes for the qualitative behaviour of a spreading flow, and conditions were found under which open channels or interior tubes were formed on slopes.

Our interest here is in the cooling of very long channel flows. Thus we take an alternative approach and consider a prescribed rigid channel. Volume fluxes and flow speeds achieved are much greater than in previous experiments with PEG extrusions and give moderate Reynolds numbers similar to those of large basalt channel flows. We observe the ways in which the flows cool and solidify at their free surface. In particular, we determine the conditions under which the down-slope channel flows either remain 'open' (with only mobile solid on the surface) or become encased beneath a solid roof to form the equivalent of a lava tube. The experiments are described in § 2 and qualitative observations are given in § 3. A detailed analysis of the experimental conditions and regime transitions is provided in § 4. The role of convection is explored in § 5 and the roles of both shear and convection are further discussed in § 6. We evaluate the relevant conditions for lava flow examples and point to similarities between the laboratory and lava flows in § 7. Our conclusions are summarized in § 8.

2. Apparatus and measurements

Our experiments consisted of sustained releases of polyethylene glycol wax (PEG, grade 600) at a constant flow rate and temperature under cold saline solutions in sloping, acrylic channels (figure 3). The channel of desired length and width was placed inside a glass tank that was larger in all dimensions: 0.4 m deep, 0.2 m wide and 4 m long. The channel was inclined at the desired angle with its lower end open and raised off the floor of the outer tank (by 49 mm or 66 mm): wax flowed down the sloping channel and fell on to the base of the outer tank, the full length of which served as a waste repository. The outer tank was initially filled with pre-chilled saline solution with a salt concentration chosen to give the desired wax–water density difference $\Delta\rho$. This solution also flooded the sloping channel to a depth of at least 200 mm. A number of channels of differing geometry were used in order to vary the channel length L and channel width W: we began with experiments in a channel 1.6 m $\times$ 80 mm, and then turned to a channel 3.0 m $\times$ 80 mm, in which most experiments were run. We also added transparent acrylic sheets inside the walls of

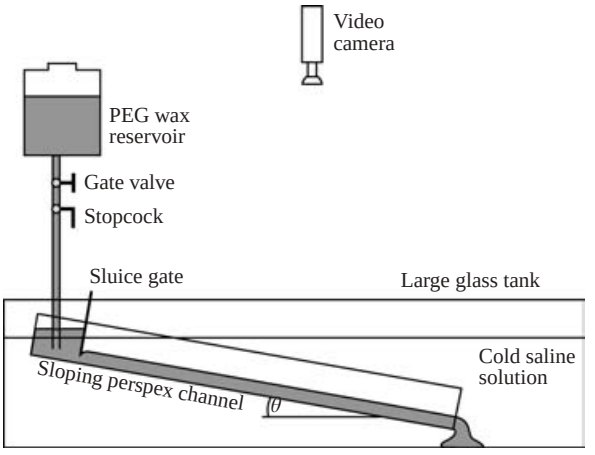

FIGURE 3. Diagram of the laboratory apparatus used for experiments with surface cooling of flows in sloping channels.

this channel to make it narrower, 2.4 m × 44 mm, and later ran a series of experiments in a wide channel 1.9 m × 150 mm. In most of the runs we used a slope of $\theta = 3.5°$. However, some runs had $\theta = 1.6°$, 3.3° or 7.0°.

The PEG supply was gravity fed via a tube from an overhead reservoir (of volume 30 l) through a stopcock and a multi-turn gate valve. The tube supplied a lock behind a sliding sluice gate placed approximately 200 mm from the end of the channel. The closed sluice gate kept the lock dry while the remainder of the channel was filled with the cold water. It also allowed the volume behind the gate to be filled with PEG immediately prior to starting a run. To begin the flow the sluice gate was slid upwards by 10–50 mm and the stopcock was opened at the same time. The height to which the gate was pulled up from the bottom of the channel was chosen to give a vent almost as deep as the PEG flow downstream, but not deep enough to allow water to flow upstream under the gate. This provided a means of generating an outflow of uniform depth and spanning the channel width, minimizing unwanted vertical and cross-channel velocities at the vent. No mixing of the wax and water could be seen, except in cases of unintentionally large initial depth of wax behind the gate; these experiments were rejected. The volume flux Q was controlled by the valves and measured by timing head loss in the reservoir. After observing the behaviour during a period of constant source flow, the flow rate was increased or decreased in order to study different flow conditions, or the sluice closed and the channel cleared for another run.

The water temperature T_a in the channel and PEG temperature T_e in the reservoir (the vent temperature) were measured immediately before starting the flow and again at intervals during and after the experiment. In many of the experiments the water temperatures were logged continuously using a computer and calibrated thermistors placed at two positions (0.2 m and 1.2 m downstream from the vent and 20 to 40 mm above the wax surface). The water temperature in the experiments was below 11 °C, which was sufficient to ensure that the slow dissolution of wax in the water had no discernible effect on the results. The wax reservoir temperature in all runs lay between 25 °C and 27 °C, and was chosen to be well above the solidification temperature T_s in order that the difference $T_e - T_s$ was known to within 10%. Most of the uncertainty in this temperature difference arose from the uncertainty in T_s. In order to find the

appropriate solidification temperature of the PEG we measured the time for formation of white solid in a thin glass tube filled with PEG initially at 24 °C and plunged into a water bath at a range of temperatures. From the results we estimated the water temperature at which this time becomes asymptotically large (i.e. much greater than one minute, which is the timescale relevant to our channel experiments). It was found previously that this asymptote lay at a temperature consistent with that at which the melt viscosity increased rapidly with decreasing temperature (Fink & Griffiths 1992). For the PEG used in the present experiments $T_s = 18.5\,^{\circ}\mathrm{C}$ to $19.5\,^{\circ}\mathrm{C}$ ($\pm 0.5\,^{\circ}\mathrm{C}$), depending on the manufacturer's batch.

A video camera mounted 2 m above the channel on a travelling gantry provided a continuous record of each experiment, from which we later measured details of the distribution of solid crust. The solid showed as white against the black base of the channel. A second video camera was in some cases used to record the flow from the side. Still photographs were taken from a camera mounted overhead and looking downward normal to the sloping base of the channel, and from a second hand-held camera at varying positions and oblique angles. Measurements of the flow depth H in many runs were also recorded from a ruler on the outside of the channel wall.

In several additional experiments we released continuous streams of dyed wax from 2 mm diameter tubes placed immediately inside the sluice gate. The tracer outlets were placed at a height such that the dye lines immediately downstream of the gate lay close to the surface of the wax and at distances from each sidewall varying between 5 mm and 20 mm (the vertical and horizontal position of the tubes were varied to reveal the paths of tracer on different streamlines originating at the sluice gate). The channel was given a white base for these runs. The streams of passive tracer provided an indication of any vertical and cross-stream motion within the flow and showed whether the flow was steady. Some of the dye tracer experiments had conditions that overlapped those of the solidifying flows (in which case solid partially obscured the tracer). Other runs had higher PEG and water temperatures so that there was no solidification, but a comparable heat flux, across the flow surface.

3. Appearance of the flows

3.1. *Classification*

The observed styles of solid crust distribution are illustrated in figures 4 and 5. There were two distinctly different regimes of behaviour. In one regime (which we refer to as 'tube'), there was a rigid solid roof over the flow for much of the length of the channel, with the flow proceeding through an encased tube beneath. In the other regime (referred to as 'mobile crust') the flow surface along the centre of the channel was covered with solid to varying extents, but remained mobile. A third class of behaviour (which we refer to as 'transitional') showed some elements of both the above regimes and was dependent on time and distance down the channel.

The 'tube' regime (figure 4*a*) occurred at small vent fluxes or low water temperatures. These conditions led to chilling of the flow surface before it could flow far from the vent. The solid crust extended from wall to wall. It was stationary in runs with lowest water temperatures and smallest vent fluxes. In many warmer cases it tended to slide against the smooth walls and move slowly down the sloping channel. However, we expect that if there had been any wall roughness, irregularities or bends in the channel, the roof would have been always locked in place. In the six runs with the coldest water (where ψ was less than about 0.35), the stagnant roof grew some distance in the downstream direction, either from the vent or from segments of roofed channel,

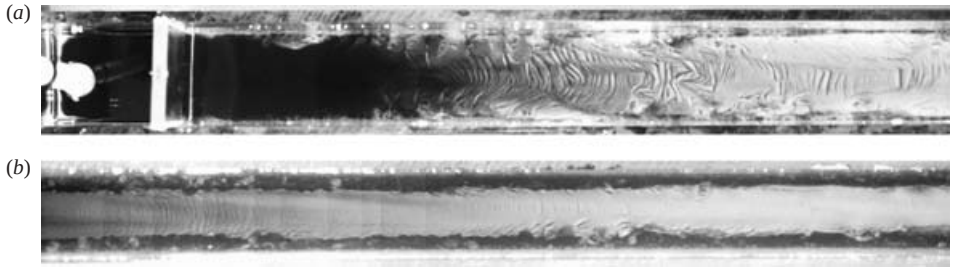

FIGURE 4. Photographs showing views from above (with optical axis normal to the inclined channel) of two runs in the intermediate-width channel ($W = 0.08$ m): (*a*) 'tube' flow under a rigid stationary crust (exp#24/5, 37 min after starting the flow, $Q = 2.5\,\mathrm{cm^3\,s^{-1}}$, $T_a = 8.5\,^\circ\mathrm{C}$, $r = 0.082$, $\psi = 1.95$, $Ra = 1.3 \times 10^5$, $\vartheta = 21.5$, visible section along channel is $x = -0.2$ to 0.68 m); and (*b*) the 'mobile crust' regime in which the solidified raft of crust along the centre of the channel is separated from the sidewalls by open shear layers in which only dispersed solid occurs (exp#19/2, 2.5 min after starting, $Q = 17\,\mathrm{cm^3\,s^{-1}}$, $T_a = 6.5\,^\circ\mathrm{C}$, $r = 0.16$, $\psi = 1.58$, $Ra = 9.0 \times 10^5$, $\vartheta = 32.9$; $x = 0.3$ to 1.2 m). In (*b*) the central crust is darker at the left partly because the illumination was non-uniform and partly because the solid was thinner close to the vent. The channel walls can be seen at top and bottom of the images. The supply tube, lock and sluice gate are included in (*a*). In all photographs, flow is from left to right.

while the flow issued from beneath the roof. For larger ψ, however, the roof began to form some distance downstream, where solid plates carried along on the flow surface had grown and become jammed. The roof then proceeded to extend in the upstream direction. In cases where the flow conditions had been approached by decreasing the vent flux, the formation of rigid roof often involved the broadening of a central strip of solid crust (formed in the mobile crust regime at higher vent flux – see below) until the solid reached the walls. Under conditions close to the limit for the tube regime (higher temperatures or larger vent flux), the rigid roof could break intermittently and temporarily expose melt flowing beneath the roof. A solid roof again formed over the break.

For larger volume fluxes and higher water temperatures solidification no longer led to wall-to-wall crust. As the surface melt moved down-slope, the surface temperature decreased from the vent temperature. In a central region of the channel width, the PEG surface solidified when its temperature fell below its solidification temperature, and crust developed. Farther down-slope from the onset of solid crust, a continuous raft of solid covered the centre of the channel (figure 4*b*, figure 5*c*, *d*, *e*). Because this crust was carried freely downstream we refer to this regime as 'mobile crust'. The distance from the vent to the onset of crust, the width of the crust and the shape of its upstream edge were steady. We used conditions that gave centreline solidification distances ranging from 0.1 m to 1 m. The thickness of the crust, as judged from its increasing opacity viewed from above, grew slowly with distance from its onset. The crust attained a maximum width within 0.1 m to 0.3 m downstream of its upstream edge, and this width remained largely unchanged along the remainder of the channel. This characteristic was particularly remarkable in the 3 m channel. Along each sidewall the surface of the flow remained free of connected solid crust in what we refer to as 'shear zones'. In many cases (figure 5*b*, and less clearly in figure 5*d*) these shear zones contained roughly circular pieces of solid ('rosettes') with widths slightly less than the width of the shear zone that rotated in the shear as they were carried downstream. Rosettes formed at positions close to the upstream edge of the central raft of crust and, in this vicinity, tended to grow with distance downstream. Further

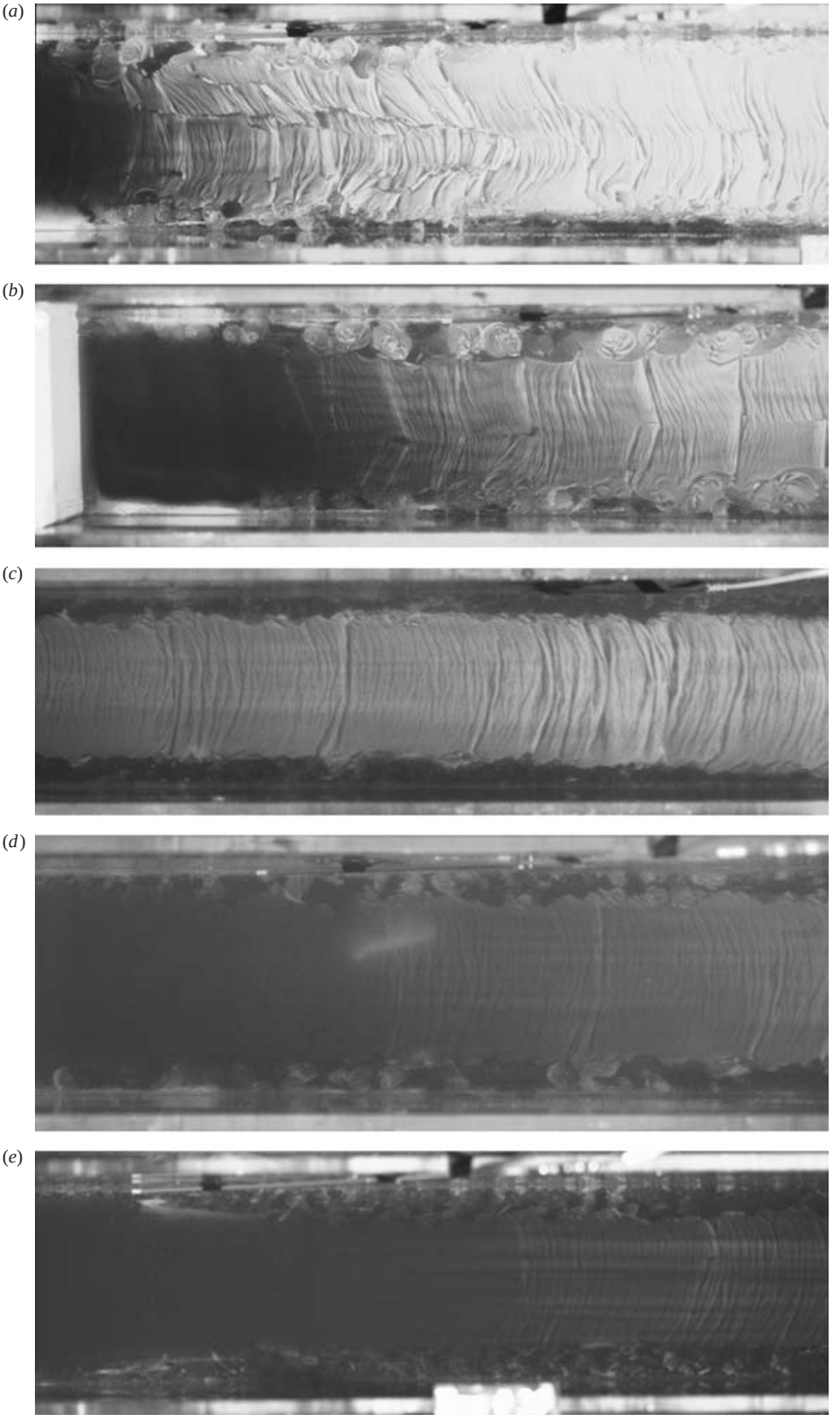

FIGURE 5. For caption see facing page.

downstream, where the shear zones were of fixed width, the solid pieces ceased to grow but developed irregular boundaries and sometimes welded to the central raft. In other runs the shear zones were dominated by finely shredded pieces of crust ('snow') rather than larger rosettes (figure 5*c*, figure 6*a*). We did not ascertain the variables governing this difference.

Within the mobile crust regime, the onset of solidification at the centre of the channel occurred farther from the vent for larger volume fluxes or higher water temperatures. The crust thickness also grew more slowly with distance down-slope, and the width of the solid raft tended to be smaller. Thus the sidewall shear zones tended to be wider. The central raft always carried fossilized compression folds formed near its upstream edge (all frames of figure 5). In many experiments the solid raft also tended to break into segments (0.1 to 0.3 m long) that proceeded to overlap, indicating a compressive stress at the surface along the full length of the channel. The compression occurred even when we judged that influences from the far downstream end of the channel were minimal. However, the raft was sensitive to conditions at the far end of the channel, and to changes in flow rate from the vent. Thus, if the vent flux decreased, the central raft adjusted by pulling apart into separate segments. Alternatively, if the crust was held up at the far end of the channel (where the strength of the solid sometimes prevented breaking of the raft as it fell into the outer tank, causing it to block the exit), upstream roof segments sometimes began to over-ride each other. Apart from these features, and the increasing crust thickness with distance, the flow and its solid crust were independent of distance down the channel. The channel length L had no obvious influence on the flow.

The 'transitional' classification was introduced for cases in which the solid rafts spanned the full width, or almost the full width, of the channel (figure 5*a*, *b*) and temporarily or locally formed a tube, but in which the flow tended to break and over-ride segments of roof. The shear zone decreased in width with distance from the vent. Solid rosettes, formed near the vent, froze onto the central crust to create a solid raft across the channel that moved steadily with the flow rather than stagnating to form a true tube. However, the presence of the solid crust apparently decreased flow rates down channel sufficiently that the flow tended to over-ride and subsume the fixed crustal segments, and could produce internal stacking of alternate solid and liquid layers. In this way the flow slowly backed up and deepened toward the vent (figure 6*d*). This transitional time-dependent behaviour was reproducible at given

FIGURE 5. Photographs showing views from above (with optical axis normal to the inclined channel) showing short sections of the wide channel ($W = 0.15$ m) for a number of runs in the transitional and mobile crust regimes. (*a*) $Q = 18.5\,\mathrm{cm^3\,s^{-1}}$, $T_a = 8\,^\circ\mathrm{C}$, $r = 0.079$, $\psi = 1.03$, $Ra = 7.3 \times 10^5$, $\vartheta = 19.9$, transitional regime with some over-riding of segments of crust, $x \approx 0.1$ to 0.7 m (exp#40/2). Apart from the over-riding and stacking (not obvious in this top view) this photograph also illustrates the wall-to-wall crust of the tube regime. (*b*) From the same run as (*a*), a view of the near-vent region, showing the 'rosette' structures, $x \approx -0.04$ to 0.56 m. (*c*) $Q = 44.2\,\mathrm{cm^3\,s^{-1}}$, $T_a = 7\,^\circ\mathrm{C}$, $r = 0.11$, $\psi = 1.15$, $Ra = 1.8 \times 10^6$, $\vartheta = 30.0$, 'mobile crust' regime with dispersed small fragments of solid throughout shear zones at all distances far from vent, $x \approx 0.6$ to 1.2 m (exp#40/1). (*d*) From the same run as (*c*), showing the near-vent region, the onset of central crust and development of the distinct sidewall zone of broken solid with small rosettes, $x \approx 0$ to 0.6 m. (*e*) $Q = 55\,\mathrm{cm^3\,s^{-1}}$, $T_a = 8.6\,^\circ\mathrm{C}$, $r = 0.11$, $\psi = 2.05$, $Ra = 2.5 \times 10^6$, $\vartheta = 59.7$, 'mobile crust' regime again showing the development of shear zones close to the vent, this time without the larger rosettes, $x \approx 0$ to 0.6 m (exp#39/1). The solid in (*e*) is more difficult to see in the photograph because it is relatively thin. The solidification pattern in (*c*) was the most common at sufficiently large values of ϑ.

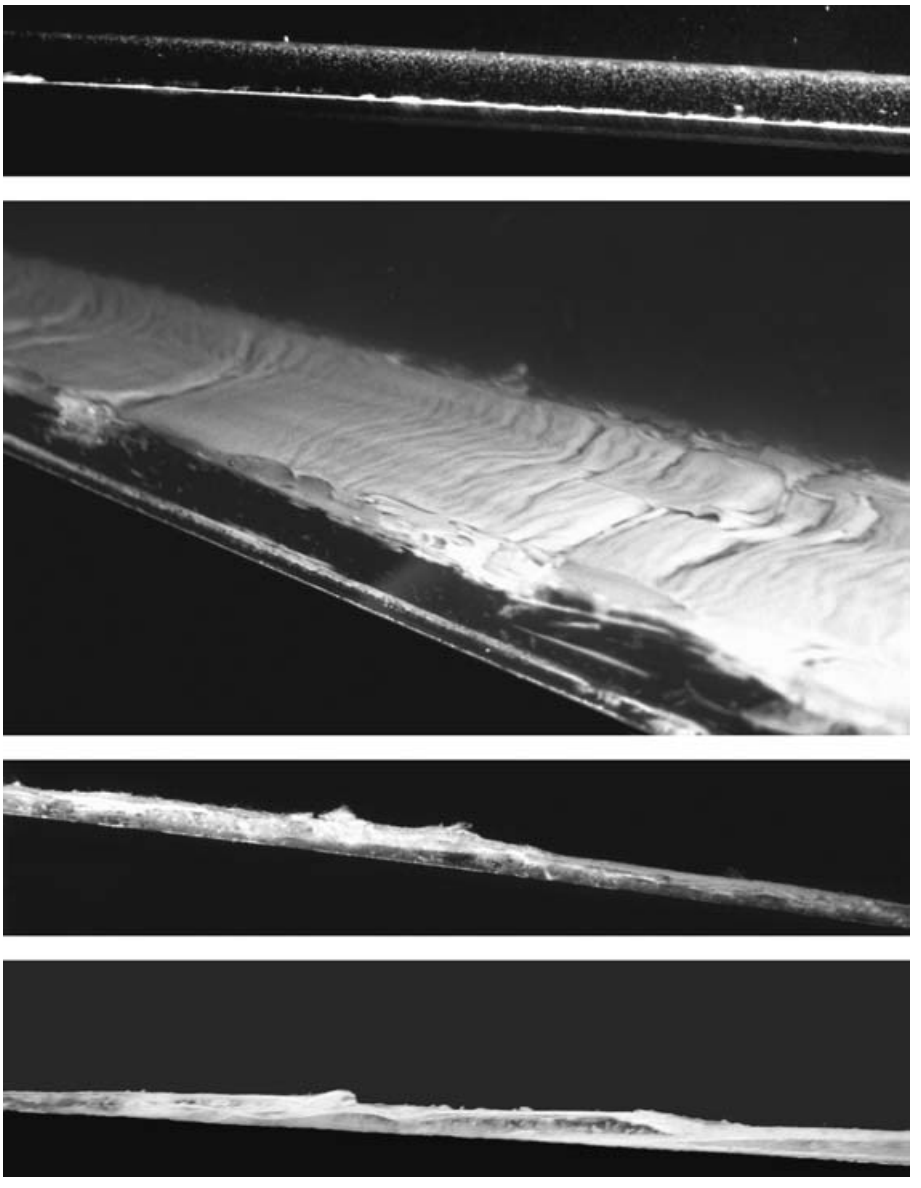

FIGURE 6. Side view photographs of solidifying flows: (*a*) a horizontal view of the mobile crust regime, showing fine dispersed solid being carried down the sidewalls of the channel, starting at the vent (exp#35/2, $W = 0.08$ m, $Q = 71.7\,\mathrm{cm^3\,s^{-1}}$, $T_a = 8.2\,^{\circ}\mathrm{C}$, $r = 0.29$, $\psi = 4.26$, $Ra = 7.3 \times 10^5$, $\vartheta = 159$, $x \approx 0$ to 0.40 m); (*b*) an oblique view of a transitional flow, but one that is also much like those in the tube regime, where solid covers the surface and there is no dispersed solid carried down the sidewalls (exp#40/5, $W = 0.15$ m, $Q = 16.7\,\mathrm{cm^3\,s^{-1}}$, $T_a = 9\,^{\circ}\mathrm{C}$, $r = 0.076$, $\psi = 1.21$, $Ra = 6.7 \times 10^5$, $\vartheta = 22.9$, of the order of 0.6 to 1.2 m from the vent); (*c*) a horizontal view of the transitional regime (same run as *b*); (*d*) a horizontal view of another transitional case showing that the flow can over-ride segments of crust and thicken upstream.

conditions and was distinct from flows travelling beneath a rigid and stagnant roof, although the latter sometimes developed surface breakouts as the result of irregular rates of flow advance.

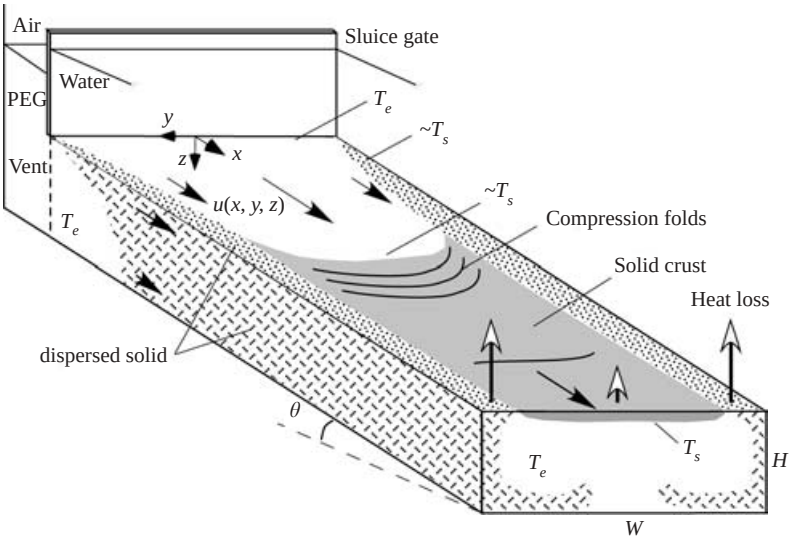

FIGURE 7. An oblique pictorial drawing noting observed characteristics of the laboratory flow in the mobile crust regime, where open shear zones persisted for the length of the channel (see figures 5*c*, 6*a*). The expected temperatures and heat flux distribution are also indicated. The down-slope distance is greatly foreshortened relative to flow depth.

3.2. *Open shear zones*

Returning to the conditions under which open sidewall shear zones were present, a notable feature was that solid phase was always visible as small ($\leqslant$2–3 mm), dispersed flakes within the shear zones, at all distances from the vent (figures 4*b*, 5*c*, 5*d*, 5*e*, 6*a*). Immediately adjacent to the vent (figures 5*d*, 5*e*; 6*a*) the highly fragmented solid could be seen only near the free surface and very close to the walls. Within 1 to 3 channel widths from the vent the sidewall layer containing the fragmented solid grew in width with distance x from the vent (figure 5*e*, figure 7). The onset of surface solidification in the sidewall boundary layers at the vent is caused by the vanishing velocity at the sidewalls and consequent cooling of the surface below the solidification temperature. However, as the horizontal gradient of velocity was largest at the walls, the surface solid was torn into small, dispersed fragments.

While the dispersed solid was carried down the channel it was also carried away from the flow surface: it travelled down the wall and then across the base of the channel towards the channel centreline. We expect the presence of uniform shear zones to depend on a matching of the continued heat loss and transport of heat from the interior to the flow surface. Thus both vertical and cross-stream transports appear to be necessary for open shear zones to persist without being covered by solid crust. We conclude that the vertical and cross-channel velocities are a consequence of thermal convection. The structure of the convection is discussed further in § 5.

It is apparent that cooling must generate both horizontal and vertical temperature gradients within the flow (figure 7). The surface temperature near the centre of the channel decreases with distance from the vent until it falls below the solidification temperature T_s, at which point solid crust forms, whereas the interior of the flow probably remains at the vent temperature T_e for a large distance downstream. Thus the vertical temperature difference applied across the melt in the central region of the channel decreases from $T_e - T_a$ at the vent to approximately $T_e - T_s$ (beneath the

solid crust) far downstream. However, considering the surface temperature of the melt rather than the temperature of the water, the temperature differences within the melt increase with distance downstream. The surface cross-channel temperature difference, on the other hand, decreases from $T_e - T_s$ near the vent (owing to the small velocities near the walls and rapid advection of the surface near the centre of the channel) to values close to zero far downstream. There the whole of the upper melt surface (whether exposed to the water or to the base of the solid crust) reaches approximately the solidification temperature.

4. Analysis of experimental results

4.1. *The basic isothermal flow*

The theoretical velocity distribution in isothermal laminar flow of depth H_0 with a free surface in a channel of rectangular cross-section, width W and slope angle θ to the horizontal can be written as (White 1991; Tallarico & Dragoni 1999):

$$u(y,z) = \frac{16}{\pi^3}\frac{g'\sin\theta H_0}{\nu_0}\sum_{n=1,3,5\ldots}^{\infty}\frac{1}{n^3}(-1)^{(n-1)/2}\left[1-\frac{\cosh(n\pi y/2H_0)}{\cosh(n\pi W/4H_0)}\right]\cos\frac{n\pi z}{2H_0}, \qquad (2a)$$

where $g' = g\Delta\rho/\rho_0$ is the (reduced) gravitational acceleration, g is the gravitational acceleration, $\Delta\rho$ is the density difference between the fluid and overlying water, ρ_0 is the density of the fluid and ν_0 is the kinematic viscosity of the fluid. In this flow the maximum velocity U_0 occurs on the surface $z = 0$ and centreline $y = 0$, and is

$$U_0 = \frac{g'\sin\theta H_0^2}{2\nu_0}\left[1-\frac{32}{\pi^3}\sum_{n=1,3,5\ldots}^{\infty}\frac{1}{n^3}(-1)^{(n-1)/2}\operatorname{sech}\frac{n\pi W}{4H_0}\right]. \qquad (2b)$$

In our experiments it is more practical to impose the total (steady) volume flux Q rather than the flow depth, but the flux can be related to the flow depth and width by

$$Q = \frac{\rho_0 g'\sin\theta}{3\nu_0}W H_0^3\left(1-\frac{384}{\pi^5}\frac{H_0}{W}\sum_{n=1,3,5\ldots}^{\infty}\frac{1}{n^3}\tanh\frac{n\pi W}{4H_0}\right). \qquad (2c)$$

In the above solution it is assumed that there is no shear stress at the free surface and that the surface is planar, with no disturbances or mixing with the overlying fluid. The solution is valid when the Reynolds number $Re = U_0 H_0/\nu_0$ is sufficiently small for the flow to be laminar and the flow length $L \gg H_0/\sin\theta$ (ensuring that buoyancy forcing due to any variation of flow thickness is overwhelmed by that associated with the bottom slope). The isothermal flow in a uniform channel, given by (2), is then described by three dimensionless parameters: the Reynolds number Re, the aspect ratio $r = H_0/W$ and the slope angle θ. A dependence on Re will be significant only at large Re or when the flow is perturbed by convective instabilities or channel irregularities. In that case the ratio of flow speed to the gravity wave speed, expressed as a Froude number $Fr = U_0/\sqrt{g'H_0}$, is also an important consideration. The free surface (which is of central importance to solidification) can support standing waves and is unlikely to remain planar when $Fr > O(1)$. However, from (2), Fr is not an independent parameter and can be written as a function of Re, r and $\sin\theta$. In this paper we consider only straight, uniform channels.

For each experimental run, irrespective of whether the flow was cooled, we calculated both the theoretical velocity U_0 and the depth H_0 for the corresponding

Variable	Symbol	Value	Units
PEG thermal diffusivity	κ	8×10^{-8}	$m^2\,s^{-1}$
PEG specific heat	c	2.49×10^3	$J\,kg^{-1}\,K^{-1}$
PEG viscosity (at T_e, given in °C)	ν	$1.5834 \times 10^{-4} \exp(1.2466 - 0.069063T_e + 3.1364 \times 10^{-4}T_e^2)$	$m^2\,s^{-1}$
PEG density (at T_e, given in °C)	ρ	$1.1264 \times 10^3 - 0.8559(T_e - 20)$	$kg\,m^{-3}$
PEG thermal expansion coefficient	α	8.56×10^{-4}	K^{-1}

TABLE 1. Parameter values for PEG 600, taken from Fink & Griffiths (1990) and Kerr (1994).

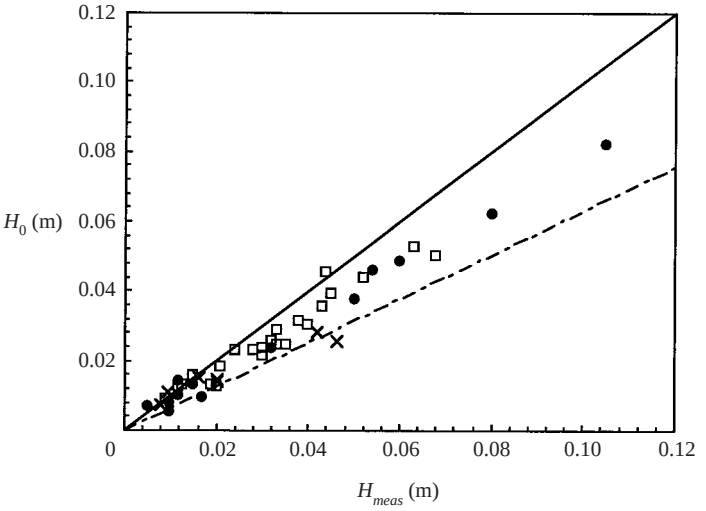

FIGURE 8. Comparison of the measured depths H_{meas} of solidifying flows and the depth H_0 predicted for the same volume flux and channel geometry but no cooling. The solid line is $H_{meas} = H_0$ (free-slip surface) and the broken line is $H_{meas} = 2^{2/3}H_0$ (no-slip surface and wide channel). Symbols indicate solidification regime: ●, tube flow with a fixed solidified roof; □, mobile crust flows in which the solid is confined to a central strip, ×, transitional flows.

simple flow with the same volume flux but no cooling. For this calculation the PEG viscosity ν_0 and density ρ_0 were temperature dependent (Fink & Griffiths 1990) and defined as those at the vent temperature. These dimensions and PEG properties (see table 1) were then used in the normalization of the variables discussed below for comparison of run conditions.

All the flows were laminar, with $Re = 0.3$–70. The apparatus was specifically designed to achieve this range of small to moderate Reynolds numbers, covering the values relevant to terrestrial basaltic lava channels (Booth & Self 1973; Lipman & Banks 1987; Cashman *et al.* 1999; Griffiths 2000). The Froude numbers lay in the range 0.1 to 0.7. There was no mixing between the PEG and the overlying water (except in a few runs with larger Re and $Fr \approx 1.0$, and these were removed from the data set). The aspect ratio ranged between $r = 0.05$ and $r = 2$ owing to the use of different channel widths and volume fluxes. The *measured* flow depths, H_{meas}, tended to be larger than H_0 (figure 8). This increased depth is attributed largely to the effect of drag exerted on the flow surface by the overlying water. Some increase in depth

may also result from a decrease of the surface velocities near the centre of the channel due to the formation of a solid raft that averaged the surface speed across the central region of the flow. The measured depths on figure 8 therefore lie between H_0 and $2^{2/3}H_0$, the latter being the predicted height of a very wide fully enclosed channel that is required to carry the same imposed volume flux.

4.2. *Dimensionless parameters for cooling flow*

Three additional dimensionless parameters are required to describe the thermal conditions for flows with surface cooling, but without solidification (Griffiths 2000). We define these as

$$\left.\begin{aligned} Pr &= \nu_0/\kappa, \\ Nu_s &= F_e H_0/\rho_0 c\kappa\,\Delta T, \\ Ra &= g\alpha(T_e - T_s)H_0^3/\kappa\nu_0. \end{aligned}\right\} \tag{3}$$

The first is the Prandtl number of the fluid, where κ is the thermal diffusivity and ν_0 is the viscosity evaluated at the vent temperature. The grade of PEG used in the present experiments has $Pr \approx 1.3 \times 10^3$; basaltic lavas have $Pr \sim 10^5$. The second parameter is the dimensionless surface heat flux Nu_s, where ρ_0 and c are the density and specific heat of the fluid at the vent temperature, $\Delta T = T_e - T_a$ and F_e is the surface heat flux when the surface is at a given temperature (say T_e). The third parameter is a Rayleigh number Ra, discussed below. Note that the Péclet number $Pe = U_0 H_0/\kappa$ (describing the rate of flow relative to the rate of diffusion of heat) and the Prandtl number are not both required because $Pe = Re\,Pr$.

When solidification is involved, an additional dimensionless parameter is the ratio of temperature differences

$$\Theta_s = (T_s - T_a)/(T_e - T_a) \tag{4}$$

(or its complement $1 - \Theta_s = (T_e - T_s)/(T_e - T_a)$, which tends to be the more convenient form to work with in setting up experiments because the most relevant values of Θ_s are close to 1). It is assumed in this discussion that latent heat effects are negligible.

Previous work with slow spreading flows (Fink & Griffiths 1990, 1992) has provided evidence that the roles of the three parameters Θ_s, Pe and Nu_s are largely captured by the single parameter ψ, defined in (1). The Péclet number governs the thickness of the thermal boundary layer at the flow surface relative to the flow depth, the temperature ratio tells us the temperature decrease sufficient to cause solidification, and the dimensionless heat flux determines the time required for this temperature decrease to occur within the boundary layer. Thus ψ is the ratio of a timescale t_s for the flow surface to reach the solidification temperature and the timescale H_0/U_0 for down-channel flow. Equivalently, it is the distance $U_0 t_s$ travelled by fluid at the channel centre line (expressed in flow depths) before onset of solidification.

Following the previous approach we have chosen to define values of ψ for channel flows based on the theoretical isothermal flow depth and velocity. The actual depth may not have a unique value and the measurement of depth for lava flows poses practical difficulties. This choice of H_0 also keeps the definition as close as possible to external variables (although H_0, U_0 and t_s are not strictly external).

The solidification timescale t_s was calculated in the manner described by Fink & Griffiths (1990) and Griffiths & Fink (1997). This timescale is based on the idealized situation of a fluid initially at uniform temperature T_e and with its surface coming into contact, from the time $t = 0$, with water at temperature T_a. A cooled surface boundary layer develops. The evolution of the surface temperature is found by assuming

purely conduction in the wax or lava flow and parameterized high-Rayleigh-number convection in the water above. We parameterize the turbulent convective heat flux F_s from the flow surface (in the water) as

$$F_s = \gamma \rho_a c_a \left(\frac{g \alpha_a \kappa_a^2}{\nu_a} \right)^{1/3} (T_c - T_a)^{4/3} \tag{5}$$

(Turner 1973), where α is the thermal expansion coefficient, subscript a denotes properties of the ambient water solution, T_c is the contact temperature at the flow surface and γ is a numerical factor that depends weakly on Rayleigh number (Denton & Wood 1979). At the large Rayleigh numbers ($Ra \sim 10^9$–10^{10}) characteristic of the convection in the experiments, an appropriate value of $\gamma = 0.14$ (noting that for heat transfer from only one boundary the constant $\gamma = 2^{4/3} C$, where C is the appropriate constant for convection between two parallel plates). The flow surface cools toward the ambient water temperature over a timescale λ. If it is assumed that heat transport to the surface within the flow is by conduction alone, this timescale is given by (Fink & Griffiths 1990)

$$\lambda = \left(\frac{\rho_0 c}{\rho_a c_a} \right)^2 \frac{\pi}{\gamma^2} \left(\frac{\nu_a}{g \alpha_a (T_e - T_a)} \right)^{2/3} \frac{\kappa}{\kappa_a^{4/3}}, \tag{6}$$

where ρ_0, c and κ are again the initial density, specific heat and thermal diffusivity of the PEG (or lava), and the contact temperature T_c is a function only of the temperature ratio Θ_s.

The timescale for onset of surface solidification is then defined as the time t_s at which T_c reaches the solidification temperature T_s. A numerical solution was obtained for t_s/λ as a function of Θ_s (Fink & Griffiths 1990). For convenience in the calculation of t_s for each and every experiment, the numerical solution for t_s/λ was approximated by a polynomial in powers of $\log \Theta_s$ that provides an excellent fit to the numerical solution (for $\Theta_s > 0.4$, Griffiths & Fink 1997):

$$\ln \frac{t_s}{\lambda} \approx -8.8694 - 40.443 \ln \Theta_s - 135.89 (\ln \Theta_s)^2 - 294.24 (\ln \Theta_s)^3 - 364 (\ln \Theta_s)^4 - 236.08 (\ln \Theta_s)^5 - 62.111 (\ln \Theta_s)^6, \tag{7}$$

and the value of t_s was found from (6) and (7).

The dimensionless parameter Ra, defined in (3), measures the tendency for convection to occur within the flow. We base Ra on the thermal expansion coefficient α for PEG or lava and the flow depth H_0, while noting that the aspect ratio r may also be of significance in determining convective heat transport from the flow interior to the surface. As discussed above, surface cooling will give rise to mean temperature gradients in both the vertical and cross-channel directions (at least in locations sufficiently close to the vent). Hence convection may, in principle, occur even when Ra is smaller than the critical value for Rayleigh–Bénard convection. However, we parameterize the convective heat flux far from the vent in terms of the vertical temperature difference between the cooled liquid surface and the hot interior of the flow. The liquid surface is constrained to lie between T_e and T_s, while the interior is assumed to remain at temperature T_e for the length of the flow. Thus we define Ra in terms of the temperature difference $T_e - Ts$.

The resulting convective heat flux F_i to the flow surface, assuming values of $Ra > 10^6$, will be given by (5) but with the material properties replaced by values appropriate to the PEG or lava and the temperature difference replaced by $T_e - T_s$. This flux can

be written in dimensionless form as

$$Nu = \frac{F_i H_0}{\rho c \kappa (T_e - T_s)} \approx \left(\frac{Ra}{R_0}\right)^{1/3}, \tag{8}$$

where R_0 is a constant (or the critical Rayleigh number in an extrapolation of the 1/3-power law to $Nu = 1$). For the Rayleigh numbers relevant to our PEG flows ($10^5 < Ra < 10^8$, see below), the appropriate value of the constant in (5) is $\gamma \approx 0.20$, or $R_0 \approx 100$ in (8) (Denton & Wood 1979). In our experiments, there was also a weak conductive heat flux into the channel walls and floor, which decreased in time from about 1/3 to 1/40 of the convective heat flux to the flow surface. In the most rapidly cooled and slowest flowing experiments (which produced tubes), this heat flux formed a thin chill layer of wax on the channel walls and floor, which was soon thermally eroded by the continuing flow (cf. Kerr 2001).

In previous lava flow modelling using PEG wax, the role of convection within the flow has been neglected and the timescale t_s was calculated assuming that heat transport to the surface is by conduction alone. Given that the predicted values of t_s are sufficiently small to prohibit the onset of convection within the distance $U_0 t_s$ from the vent (t_s was of the order of only a second for the laboratory wax models and only tens of seconds for lava flows, where cooling is by radiation; Griffiths & Fink 1992*a*), we retain these definitions of t_s and ψ. However, an important result of the present work is that channel flows, by virtue of their large length compared to depth, are influenced by convection and thus their behaviour depends additionally on Ra.

When evaluating the dimensionless parameters for each experiment, we allowed for the temperature dependence of PEG density and viscosity (Fink & Griffiths 1990; table 1). The density varied linearly with temperature and hence the expansion coefficient was constant ($\alpha = 8.56 \times 10^{-4}\,\mathrm{K}^{-1}$ over the temperature interval T_s to T_e). We also took into account the dependence on both temperature and salinity of the density, thermal expansion coefficient (Ruddick & Shirtcliffe 1979) and viscosity (Washburn 1926) of the salt solution. The density and viscosity were evaluated at the ambient temperature and salinity, whereas the expansion coefficient (relevant to the amount of buoyancy in a thermal boundary layer in the water) was evaluated at the average of T_a and T_s. Fixed values were used for the thermal diffusivities and specific heats of the water solution (Washburn 1926) and PEG (Kerr 1994; table 1).

Figure 9 shows the range of Ra and r for our experiments. Aspect ratios near 1 were achieved in the narrow ($W = 40$ mm) channel, whereas $r < 0.1$ was achieved mainly in the widest channel ($W = 150$ mm). The range of Rayleigh numbers, $10^5 < Ra < 10^8$, was achieved almost entirely by changing flow depth H_0 through selection of the volume flux and one of three different channel widths. The large-Rayleigh-number parameterization of (5) and (8) is appropriate. When the observed patterns of solidification are classed into tube and mobile crust regimes, we find that the behaviour is not uniquely determined by the parameters r and Ra.

4.3. *Flow regimes*

A range of values for ψ was achieved primarily through variation of volume flux (which changes flow speed U_0 and flow depth H_0) and water temperature T_a. When the same experiments as shown in figure 9 are replotted in the ψ–Ra space (figure 10), experimental conditions giving each of the two regimes are clearly separated. For each value of Ra, tube behaviour is found at small values of ψ and mobile crust occurs when ψ is large. The transition between the regimes occurs at a smaller value of ψ for larger Ra. That is, when convection is expected to be more active within the wax

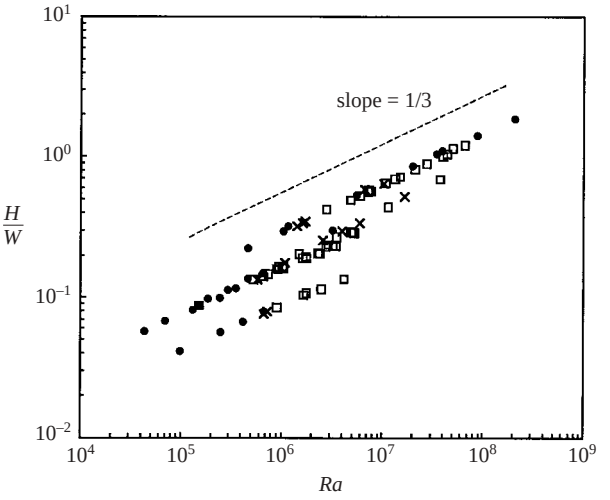

FIGURE 9. The experiments in aspect ratio – Rayleigh number space with their classifications as tube flow (fixed solidified roof, ●); mobile crust flow (solid is confined to a central strip, □); and transitional flow (×). The range of both r and Ra in each channel was achieved through variation of flow depth, whereas the three lines of data arise from the three channel widths.

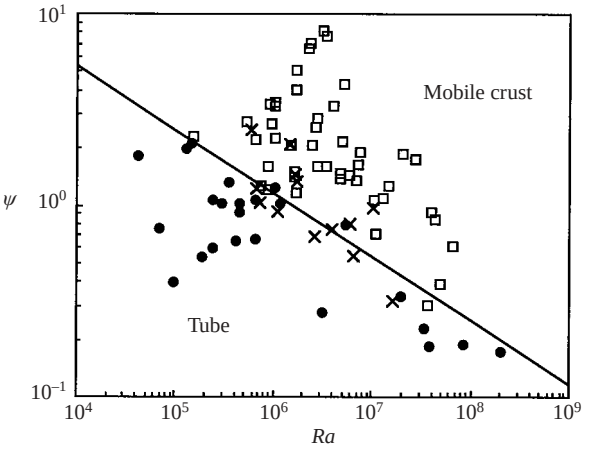

FIGURE 10. The experiments in ψ – Rayleigh number space, along with their classifications as tube flow (●), mobile crust flow (□), and transitional flow (×). Runs with bottom slopes of $\theta = 1.6°, 3.5°$ and $7°$ are included. The empirical boundary between the tube and mobile crust regimes is given approximately by $\psi = (25 \pm 5)(Ra/R_0)^{-1/3}$ with $R_0 = 100$ (solid line).

flow, the formation of a rigid roof across the whole channel is increasingly limited to smaller shearing rates U_0/H_0 and larger surface solidification times t_s (higher water temperatures and higher vent temperatures). The transition is closely defined by the results and lies at

$$\psi = (25 \pm 3)(Ra/R_0)^{-1/3}. \tag{9}$$

The experiments in which behaviour was classed as transitional lie across a broad range but tend to cluster near the above transition.

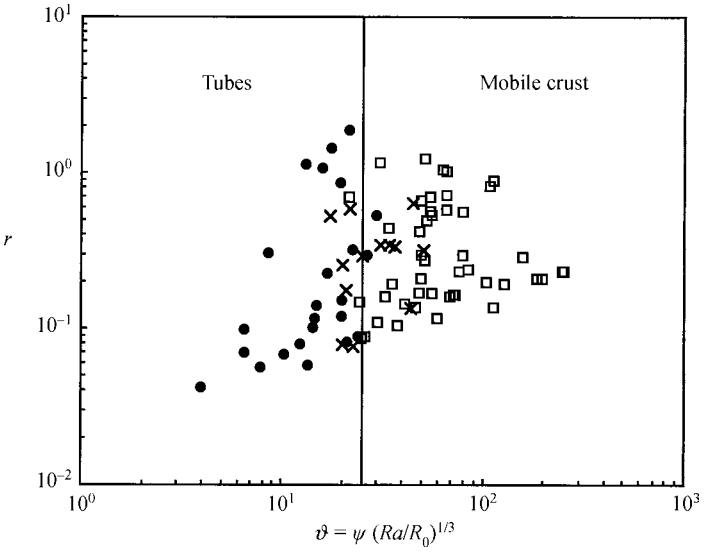

FIGURE 11. Classification of flow regimes in aspect ratio – ϑ space. The vertical line at $\vartheta = 25$ corresponds to the transition boundary shown on figure 10. This plot confirms that the flow regime is independent of the aspect ratio to within experimental uncertainty and reinforces the *Ra* dependence seen in figure 10. Symbols are as in figures 8–10.

By representing the results of figure 10 in terms of the combined parameter

$$\vartheta = \psi(Ra/R_0)^{1/3} \tag{10}$$

and plotting ϑ against r for each case (figure 11), we confirm that there is no discernible dependence of behaviour on the aspect ratio. Thus the qualitative style of solidification, at least in our PEG flows under cold water, is given solely by the conditions:

$$\left.\begin{array}{l} \vartheta < 25 \rightarrow \text{tube}, \\ \vartheta > 25 \rightarrow \text{mobile crust}. \end{array}\right\} \tag{11}$$

4.4. *Fraction of surface with crust*

The whole of the flow surface, from the vent to the far end of the channel, became roofed with a solid crust (formed a tube) for ϑ far below the transition value and after a sufficient time had elapsed. When conditions were closer to the transition, and still in the tube regime, sections of the channel length formed solid crust, with the flow either entering the tube from a region of relatively little crust on the upstream side, or emerging from beneath the rigid crust in an area of exposed melt downstream of the tube. We did not obtain quantitative information on the thickness of surface solid in the 'tube' regime.

In the mobile crust regime the width d_c of the central strip of solid crust and the complementary width d_s of the sidewall shear regions were well-defined properties of the flow. Data for the width d_c, shown in figure 12, are consistent with a simple function of ϑ when $\vartheta > \vartheta^*$: crust width decreases with increasing vent volume fluxes and increasing vent or water temperatures. Our definition of the tube regime implies that $d_c/W = 1$ at the transition $\vartheta = \vartheta^* = 25$. Results from the three different channel widths support the scaling of d_c with channel width W.

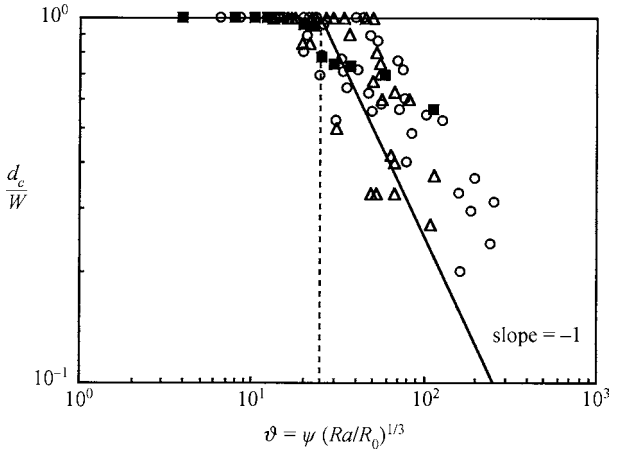

FIGURE 12. The width d_c of the central raft of mobile crust normalized by the channel width W and plotted as a function of ϑ for the three channel widths: △, $W = 40\,\text{mm}$; ○, $W = 80\,\text{mm}$; ■, $W = 150\,\text{mm}$. The solid line is given by (18) and the broken line is the regime transition $\vartheta = 25$. All runs with $d_c/W = 1$ are classed as tubes or transitional in figures 10 and 11.

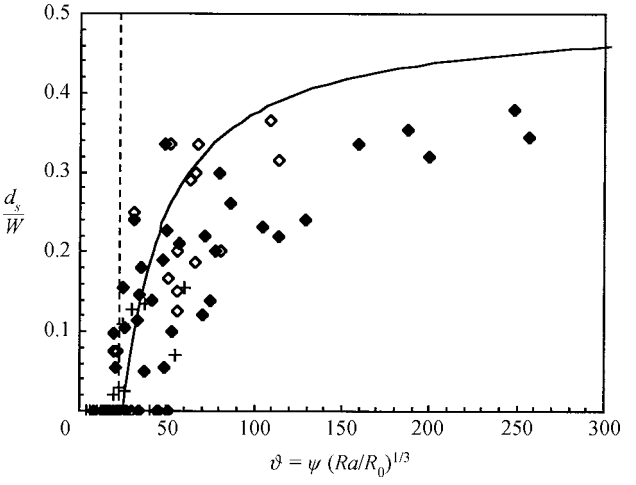

FIGURE 13. The width d_s of the open shear zones normalized by the channel width W and plotted as a function of ϑ. Runs have been placed into three bins according to their aspect ratio r: +, $r < 0.125$; ◆, $0.125 < r < 0.5$; ◇, $r > 0.5$. There is no significant dependence on r. The solid line is given by (18) and the broken line is the regime transition $\vartheta = 25$. All runs with $d_s = 0$ are classed as tubes or transitional in figures 10 and 11.

The channel aspect ratio might be expected to play a role in the width of solid crust through its influence on the cross-channel velocity profile. The profile changes from parabolic for deep flows (a linear variation of shear stress over the scale W), towards a more uniform velocity for shallow flows, where shear is concentrated within distances of order H from the sidewalls. Hence we plot in figure 13 the normalized width of the open shear zones and separate the data into three bins according to aspect ratio. Again, the transition from tube flow at $\vartheta = 25$ marks a limit, where $d_s = 0$. The shear zones become wider for larger ϑ. The data reveal no significant differences in d_s/W

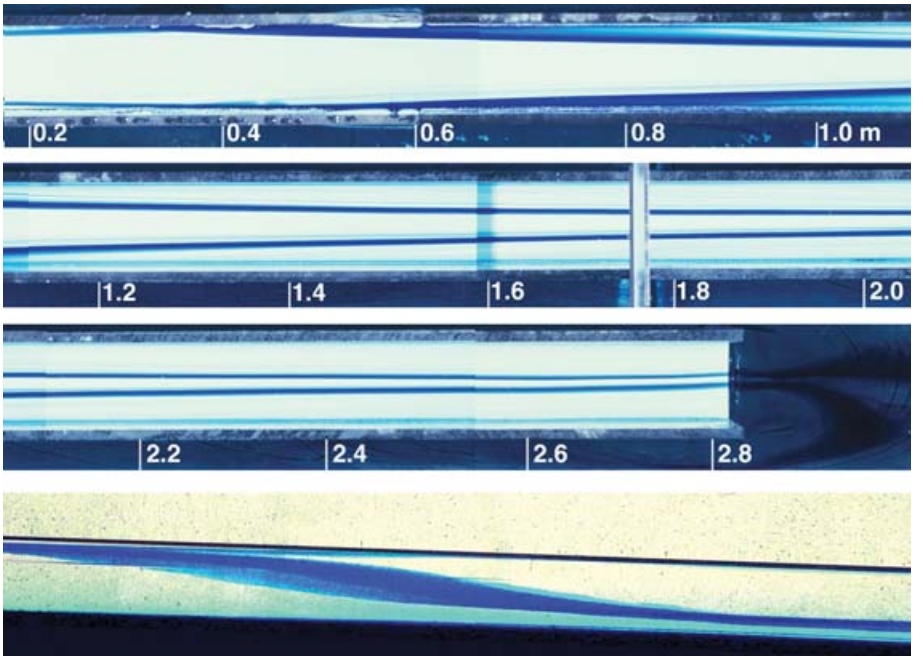

FIGURE 14. Photographs of passive dye tracer injected close to the flow surface and sidewalls in the vent, for a case with no solidification but comparable surface heat flux: (*a*) top view of the 3 m long channel cut into three contiguous segments (the vent was at $x = 0$, scale is in m); (*b*) side view of the region where the dye streams in (*a*) are closest to the sidewall. Both streams contribute to the image in the side view and an attempt was made to site the tubes in identical positions, though this was not precise. The dye marks steady streamlines. The streams at the left are adjacent to the flow surface (dark line), at the right they are close to the bottom of the channel. ($T_e = 30.0\,^{\circ}\mathrm{C}$, $T_a = 22.0\,^{\circ}\mathrm{C}$, $Q = 19.3\,\mathrm{cm^3\,s^{-1}}$, $\theta = 1.9\,^{\circ}$, $W = 80\,\mathrm{mm}$, dye inlets $8 \pm 2\,\mathrm{mm}$ from walls).

between flows having small and large aspect ratios. An explanation for the presence of open shear zones is given in § 6.

5. The role of convection

The experiments with dye tracers clearly showed the presence of cross-channel and vertical flow resulting from surface cooling. As seen in figure 14, the dye tracer leaving the vent was carried toward the wall near the flow surface, curving more sharply toward the wall as it approached the wall, as would be expected in the presence of horizontal shear with the velocity vanishing at the wall. The dye streams then moved downward close to the wall, forming a steeply inclined stream (figure 14*b*) owing to relatively slow downstream motion in the boundary layers. Near the base of the channel the streams moved away from the sidewall and toward the centre of the channel while being carried far downstream. The dye streams were stationary in time, and therefore marked streamlines of the flow. The location of the dyed streamlines depended sensitively on the location of the injection tubes. The distance downstream at which they made their closest approach to the wall (0.2 to 0.8 m from the vent) and their closest proximity to the wall (less than 5 mm) both increased when the tubes were moved farther from either the wall or the flow surface. At the same time, the

height of the dye lines above the base and their proximity to the channel centreline far downstream increased.

In runs with solidification the dye tracer revealed the same behaviour. However, photographs are less clear because the dye tends to be obscured by the surface solid. In addition, there appeared to be slightly greater dispersion of the tracer streams as a result of small-scale disturbances in the flow associated with solid fragments. In a control experiment in which the wax and water were both at 21 °C, so that there was no cooling, the dye streams showed no cross-channel motion. Instead, the streamlines were precisely parallel to the sidewalls, flow surface and base. Hence we conclude that all cross-channel and vertical motions were a result of cooling, and that solidification did not lead to further qualitative modifications of the streamline pattern.

The strong vertical and horizontal shears in the basic channel flow are expected to have a great influence on the structure (and possibly affect the heat transport) of the thermal convection. The flow pattern is also likely to be affected by the non-uniform thermal boundary conditions at the flow surface. However, the details of the convection have yet to be investigated. There have been many studies of convective instabilities in plane Couette flow with the lower horizontal boundary heated and the upper horizontal boundary cooled (Ingersoll 1966*a*), and of the effects of an applied uniform shear between two horizontal planes on high-Rayleigh-number thermal convection (Ingersoll 1966*b*; Richter & Parsons 1975; Domaradzki & Metcalfe 1988; Clever & Busse 1992). The flow is generally described in terms of the Rayleigh, Prandtl and Reynolds numbers, and it was shown that shear organizes convection into rolls oriented parallel to the direction of the forced flow, while suppressing transverse rolls. A situation more relevant to the present problem is the stability of flow down a wide inclined plate, or through a slot between two wide inclined planes, with the lower plate heated in each case. Here longitudinal rolls align with the stream, and the flow may be described in terms of Rayleigh and Prandtl numbers and the slope angle (Hart 1971). In this case, the buoyancy flux (due to base heating) was applied at the no-slip boundary and could be made sufficiently strong, relative to the down-slope flow, to force up-slope motion near the base. This convective style contrasts with the present case, where the negative buoyancy flux (due to surface cooling) was applied at the stress-free boundary and could only serve to increase the down-slope flow (though conditions were such that this effect was negligible). Finally, the effect of a non-uniform temperature distribution along the horizontal base of a shearing flow at high Rayleigh numbers has been investigated numerically (Walton 1985).

Two unique characteristics of cooling (but not solidifying) open channel flows are the application of the buoyancy flux at the stress-free surface and the finite channel width (which implies horizontal velocity gradients comparable to the vertical gradients). When the surface solidifies, it modifies the thermal boundary conditions for the fluid beneath and creates an upper boundary to the fluid that is no longer stress-free. Here the crust can modify the flow beneath, while flow stresses may break the solid apart. In this paper we simply observe that the resulting convection was highly organized into two counter-rotating rolls aligned with the stream, with downwelling of cooled liquid in a narrow boundary layer at each sidewall of the channel and a broader upwelling in the central region of the channel. The flow was in most cases steady. In one experiment at high temperatures (no solidification) there was evidence that this steady two-roll structure was breaking down, with one or more additional downwelling plumes appearing in the central region far downstream (at $x > 1.5$ m). These were quasi-linear features, again largely aligned with the mean flow

direction, but they also exhibited some waviness and unsteadiness, not unlike that observed in flow down a heated incline (Hart 1971).

6. Discussion of solidification with shear and convection

In this section we discuss two processes that underlie the complex combined roles of mechanical and thermal effects in governing the surface solidification. We present hypotheses that begin to provide an explanation of the experimental results, but which will require further theoretical and experimental development.

6.1. *Effects of thermal convection*

The presence of organized thermal convection in the laboratory channel experiments is clear. The results also provide strong evidence that the convection influences the solidification regime and the width of the open shear zones. This influence can be attributed to the convective heat flux from the flow interior to the flow surface, where it decreases the rate of cooling (relative to that calculated by assuming conduction alone) and extends the time taken for the flow surface to reach its solidification temperature.

The heat transport problem involves two convecting layers and we seek to describe the cooling of the flow surface to temperature T_s when the two layers come into contact. We are not concerned with the temperature evolution within the bulk of the fluid, because this occurs over a much longer timescale and larger down-channel distance. In detail the solution for surface temperature in the vicinity of the vent will include the development of a conductive thermal boundary layer and a modification of the conductive profile near the surface where convection begins at some distance from the vent. Further down-channel, convection is well established and we regard the process there as one of surface cooling and solidification as convection brings fresh melt from the interior to the surface. We can take advantage of the fact that viscous boundary layers (if there are any, given that Re is only moderate) are much thicker than the thermal boundary layers ($Pr \gg 1$) and of the observation that the time t^* required to establish the thermal boundary layer (of thickness δ) by conduction is much greater than the timescale t_s for conductive cooling to T_s at the surface. (Here $\delta \approx H_0(Ra/R_0)^{-1/3}$ is the thermal boundary layer thickness characteristic of high-Rayleigh-number convection and $t^* \sim \delta^2/\kappa$; for the PEG flows we estimate that $\delta \sim 1$ mm and $t^* \sim 12$ s, whereas $t_s \sim 1$ s.) Direct effects of shear and convection on conductive cooling immediately adjacent to the surface are therefore negligible and the previously defined timescale t_s (Fink & Griffiths 1990) is relevant. However, this does not explain the role of convection.

In steady channel flow, convection continuously flushes away the chilled surface of the flow, replacing it with hot interior melt and thereby maintaining the surface at a temperature between that of the flow interior and ambient water temperature. This temperature must be close to T_s. When the flushing is too slow, the surface freezes and a complete rigid crust develops. Thus an important parameter is the convective heat flux from the interior to the surface, which is given by (5) (with water properties replaced by PEG properties) or, in dimensionless form, by (8). Qualitatively, the value of Ra at which the surface freezes over must be dependent on the thermal characteristics of the flow and the surface heat flux, and these are encompassed in the variable t_s. The empirical result is that a transition from mobile central crust to tube formation is given by (9), which can alternatively be expressed as $Ra = 1.56 \times 10^6 \psi^{-3}$. A prediction of this functional form may require knowledge of the additional role of

shear, as discussed below. However, we note that the empirical form of (9) follows directly from the simple hypothesis that the rate of surface solidification on a flow undergoing large-Rayleigh-number convection is, like the heat flux, independent of the flow depth (since H_0 cancels from the right-hand side of (10)). This leaves the thermal boundary layer thickness δ as the relevant length scale and the definition of ϑ reduces to $\vartheta = U_0 t_s/\delta$.

6.2. *Effects of shear*

The experiments indicate that the horizontal gradients of down-channel velocity are of primary importance in maintaining crust-free zones (which we refer to as open shear zones) near the channel walls. The shear zones are wider for larger velocity gradients and larger solidification timescales t_s. Here we hypothesize that solid crust is able to develop only where the timescale $(\dot{\varepsilon}_s)^{-1}$ for surface shearing in the cross-channel direction y is sufficiently large compared to the timescale t_s for surface solidification. Thus solid can thicken and gain strength as a connected crust, despite the shear stress, only where

$$\dot{\varepsilon}_s t_s < \beta^*, \tag{12}$$

with β^* a numerical constant.

Convective transport of heat to the surface in the open shear zones is also essential for maintaining the observed pattern of solidification and crust distribution for a large distance down the channel. Without continuous replenishment of hot liquid to the surface, the surface temperature must eventually fall so far below the solidification temperature that crust will form despite the horizontal shear. Crust will then overtake the open shear zones. Transport of heat by thermal convection within the flow, on the other hand, can lead to an equilibration of the surface temperature in the side-wall shear zones and solidification patterns that are steady and quasi-invariant with distance down the channel. Over still larger down-channel distances (well beyond those considered in these experiments) the cooling will slowly reduce the temperature of the interior of the flow, and a strictly invariant thermal state and crust distribution cannot occur. Thus we consider the quasi-invariant state that develops many flow depths away from the vent (and which, in our experiments, persists all the way to the far end of the channel).

As a first attempt to analyse the role of shear, we examine the implications of our simple hypothesis above. For the case of parallel flow in the x-direction, our hypothesis (12) becomes that surface crust cannot form at locations where

$$u_y(y, z = 0) t_s > \beta^*. \tag{13}$$

Here u_y is the cross-stream derivative of the channel velocity, the flow surface is at $z = 0$, and we will find an empirical value of the constant β^*. Using (13) in (1) to replace the solidification timescale t_s, we obtain an inequality relating the local velocity shear at the flow surface and the global dimensionless parameter ψ:

$$u_y(y, 0) > \frac{\beta^*}{\psi} \frac{U_0}{H_0}. \tag{14}$$

For a given ψ no surface crust will form at positions where the local velocity gradient is large enough.

We observe that the crust-free shear zones are limited to the vicinity of the sidewalls and vanish (leaving tube flow) at the critical condition $\psi = \psi^* = \vartheta^* (Ra/R_0)^{-1/3}$, where

ϑ^* is a constant. Hence

$$\beta^* = \vartheta^* \left(\frac{Ra}{R_0}\right)^{-1/3} \frac{H_0}{U_0} u_y(W/2, 0). \tag{15}$$

Rewriting (14), the surface is predicted to be free of crust at locations where

$$\frac{u_y(y, 0)}{u_y(W/2, 0)} > \frac{\vartheta^*}{\vartheta} = \frac{\psi^*}{\psi}. \tag{16}$$

A relatively simple case is laminar flow in channels of rectangular cross-section for deep flows or narrow channels ($r \gg 1$). Then the surface velocity ((2a), with $z = 0$) reduces to

$$u = U_0(1 - 4y^2/W^2) \tag{17}$$

and $u_y(y, 0) = -8U_0 y/W^2$. Substitution into (16) gives the location of crust-free surface as $y/W > 1/2(\vartheta^*/\vartheta)$, which implies a central crust width d_c and complementary shear zone width d_s given by

$$\frac{d_c}{W} = \frac{1}{2}\frac{\vartheta^*}{\vartheta}, \quad \frac{d_s}{W} = \frac{1}{2}\left(1 - \frac{\vartheta*}{\vartheta}\right). \tag{18}$$

Note that convection within the flow is predicted to influence the crust and shear zone widths because the Rayleigh number enters in the equation for ϑ, whereas $\vartheta*$ is a constant.

The measured crust and shear zone widths shown in figures 12 and 13 are consistent with (18). In particular, the widths scale with channel width W, and $d_c \sim \vartheta^{-1}$. The shear zone width increases with ϑ at large ϑ, but the change is gradual and is consistent with approach to the asymptote $d_s \to W/2$. Surprisingly, there is no apparent dependence of these normalized widths on the aspect ratio of the flow. Furthermore, if we take (18) as a description of the trend for all width measurements at $\vartheta > 25$, then the normalized widths are also independent of flow depth (because H_0 cancels from the definition of ϑ).

The measurements of crust width show a large scatter, which we attribute to both uncertainties in measurement and the nature of the process. In some cases the measurement was necessarily an average along the channel owing to irregularity of the edges of the central crust, and in some cases there was a fluctuation of crust width with time. There appeared to be more than one process controlling the crust width, although we have not determined the dependence on flow conditions: in some experiments the edges of the central crust were straight and stable, in others solid pieces were torn from the edges of the central crust, leaving irregular edges and crustal fragments rotating in the shear. This phenomenon appeared similar to the formation of 'rosettes' (rounded pieces of surface crust) near the upstream edge of the central crust. These observations suggest that, under some conditions, the shear prevented crust formation wherever velocity gradients satisfied (14), while under other conditions, excess solid crust developed and was then broken away by the shear.

7. Comparisons with lava flows

Although observations of active lava flows are largely qualitative because of difficulties in making direct measurements in the field, flow parameters have been determined for some well-documented recent eruptions (e.g. Lipman & Banks 1987; Neal *et al.* 1988; Calvari *et al.* 1994; Kauahikaua *et al.* 1998; Cashman *et al.* 1999).

Lipman & Banks (1987), in particular, provide a detailed description of the 1984 eruption of Mauna Loa volcano, Hawai'i, which includes photographs that illustrate both stable crusts on open channel flows and changes in the width of the stable crust with changing flow conditions.

In general, crust-free shear zones are confined to mature (well-developed) channels that permit rapid transport of lava with relatively little solidification despite a large heat flux (figures 1, 15). Both marginal shear zones and inferred plug flow are common. Convective motions within lava channels are also observed but rarely described in detail. Perhaps the best description of convective motions is that of Booth & Self (1973) in flows produced during the 1971 eruption of Mt. Etna (figure 15*b*). Booth & Self attributed the observed 'twin spiral motion' to the combined effects of drag in sidewall shear zones and possible thermally driven convection.

Lava tube formation has been extensively described for recent eruptions at Kilauea Volcano, Hawai'i and Mt. Etna, Sicily (e.g., Guest, Underwood & Greeley 1980; Guest, Wood & Greeley 1984; Greeley 1987; Hon *et al.* 1994; Peterson *et al.* 1994; Calvari & Pinkerton 1998; Kauahikaua *et al.* 1998). Most important for tube formation are steadiness and duration of flow, with lava flux, lava rheology, and topography also playing a role. In general, lava tubes form when flow is steady over long time periods. Tubes form more readily at low volumetric fluxes and on low-gradient slopes.

Documentation of open channel flows from Mauna Loa, Hawai'i (Lipman & Banks 1987) and Mt. Etna, Sicily (Calvari *et al.* 1994) provides a quantitative basis for comparing experimental results with channel dimensions, flow rates, and dimensionless parameters estimated for active basaltic lava flows. In general, basaltic lava flows are well-described by the experimental conditions described in this paper. The channels are generally much longer than they are wide, and wider than they are deep. Depth is the most difficult channel parameter to measure for active flows, and is commonly estimated by measurements of drained channels. It appears that channel aspect ratios (H/W) rarely exceed 1 and are commonly between 0.5 and 0.05. Open channel flows have large surface heat fluxes and therefore cool and crystallize during transport away from the vent. Hence flow parameters vary greatly along the flow length. For example, channel velocities vary from greater than $15\,\mathrm{m\,s^{-1}}$ at vigorous Mauna Loa vents to $0.1\,\mathrm{m\,s^{-1}}$ at sluggish flow fronts. Flow velocities of sluggish Etna lavas may be as low as $0.01\,\mathrm{m\,s^{-1}}$. Corresponding values of Re vary from order 300 at Mauna Loa vents to less than 5 for most Etna flows. Our estimates of Ra in Mauna Loa flows also vary with distance along flow, from greater than 10^7 in proximal regions to less than 10^6 in distal channels; higher viscosity and lower temperature Etna lavas probably have Ra values near the lower end of the Hawaiian range, but probably greater than 10^5.

To relate the experiments directly to observed flow parameters we must calculate values of t_s, ψ and ϑ. Solidification timescales (t_s) are largely dependent on the eruption temperature T_e and the solidification temperature T_s, which for rapidly cooled flow surfaces is taken to be the glass transition temperature (Griffiths & Fink 1992*b*). On average, $t_s \sim 10\,\mathrm{s}$ seems a reasonable estimate for $1100\,^\circ\mathrm{C} \leqslant T_e \leqslant 1150\,^\circ\mathrm{C}$ and $T_s = 810\,^\circ\mathrm{C}$ (Ryan & Sammis 1981). Using these values we infer that $0.1 < \psi < 50$ describes most channelized basaltic lava flows, as does $5 < \vartheta < 3000$. These parameters ranges are well-covered by our experiments (figures 10, 11). Direct comparison of observed and predicted shear zone widths is, unfortunately, precluded by the absence of either direct measurements of shear zone widths or adequate photographs of channel surfaces at locations where flow parameters were measured. However, it is clear that there is a qualitatively similar pattern of surface solidification and

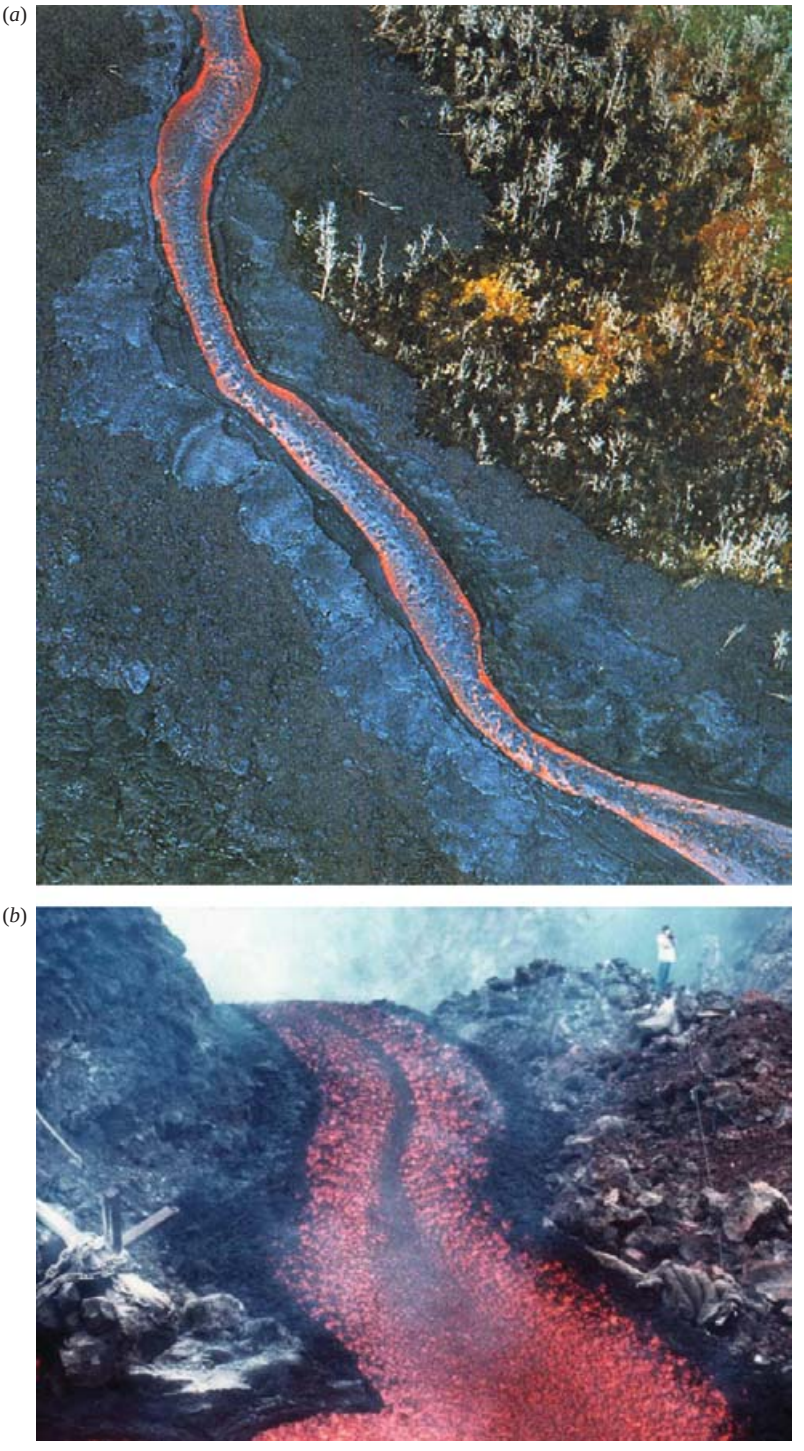

FIGURE 15. Photographs of channelized lava flows illustrating the presence of solid (dark material) along the centre of the channels and incandescent melt exposed along the edges: (*a*) a 10 m wide lava channel on Kiluaea Volcano, Hawai'i, during overflow from Mauna Ulu, February 28, 1972 (from Tilling *et al.* 1987); (*b*) a smaller flow several metres wide on Mt Etna, 23 May 1992 (note the person at upper right for scale); photo by G. Scarpinati, from *Italy's Volcanoes: The Cradle of Volcanology*, by B. Behncke, see http://boris.vulcanoetna.com.

of exposed melt in side shear zones in lava channels as in the laboratory flows. Station descriptions in Lipman & Banks (1987) describe channels as "choked with viscous debris" (i.e. close to forming a tube) in cases where we estimate $\vartheta \sim 30$–100. Additionally, Etna lava flows, with generally low values of ϑ, formed tubes when flow duration exceeded several days. Therefore we conclude that the general patterns of flow behaviour are sufficiently similar that r and ϑ should provide a useful parameterization of crustal coverage (and thus cooling conditions) during channelized flow, subject to examination of the influence of channel irregularities.

8. Conclusions

For laminar flow in uniform sloping channels, with surface cooling and solidification, there are critical conditions delimiting flows that develop an internal channel covered by a rigid solidified roof from those that maintain some crust-free surface and free down-slope advection of the surface solid. The transition occurs at a fixed value of the dimensionless parameter ϑ, which includes both thermal and flow conditions. Near the sidewalls the flow undergoes strong horizontal shearing, and for $\vartheta > 25$ this shear maintains two relatively crust-free shear zones bounding a central region of solid crust. Solidification proceeds within the shear zones but forms only small dispersed fragments of solid, which are carried by the flow. The effect is a 'snow' of solid suspended in the liquid. For $\vartheta < 25$ the shear rate is insufficient to prevent the development of solid skin at the surface, even close to the sidewalls where the shear is largest, and a rigid roof develops across the full width of the channel.

Vertical and cross-stream transport is an essential component of the laboratory flows. It results from organized thermal convection in two steady streamwise-oriented rolls. We have parameterized the convection in terms of the characteristic vertical temperature difference (between the surface solidification temperature and the interior or vent temperature). However, convection may also be forced by lateral temperature differences across the surface, especially near the vent where the surface temperature at the centre of the channel is high (close to the vent temperature) while that in the slow-moving wall boundary layers is at or below the solidification temperature. One of the most noticeable results of convection is the transport of finely dispersed solid down the sidewalls and across the base of the channel. We hypothesize that the convection is critical to the maintenance of the crust-free shear zones over large down-channel distances at large ϑ, and thus modifies the minimum volume flux or vent temperature allowed before a tube will form. When the shear rate near the walls cannot overwhelm the rate of solidification at the surface, or the convective transport of heat from the interior to the flow surface cannot match the surface heat loss, the solid crust can cover the full width and becomes fixed. The flow under these conditions is confined to an interior channel in which it experiences different mechanical and thermal boundary conditions, and its upper boundary is relatively well-insulated against cooling. Under conditions well below the transition to the tube regime, the rigid roof can develop in other ways, such as by growing downstream from the vent.

The laboratory experiments reveal the growth of compression folds in the region of early crust development, where the solidifying skin can be deformed by the imposed viscous stresses. Farther downstream, for $\vartheta > 25$, the central raft of solid crust is rigid and covers a significant fraction of the width of the channel, altering the velocity distribution there. This crust therefore travels more slowly than the central surface velocity upstream of the crust, causing the deceleration and folding of the surface.

The folding and later deformation of the crust is sensitive to other effects that lead to convergence or divergence of the streamwise velocity. We find that the compression can readily be changed to extension (and pulling apart of the solid crust) by a decrease in the vent volume flux.

A number of aspects of the problem warrant further study. The details of solidification and crust formation in a simple shear flow will need to be elucidated, as will the structure of convection in channel flows. The overall effect of these processes on the flow (and hence on the final length of a lava flow) will be through the slow cooling of the flow interior over large distances. Thus the heat loss through the partially solid and partially molten surface needs to be described more accurately. In addition, a range of channel irregularities and variations in the source conditions, which are not captured in the present experiments with a uniform straight channel and constant vent volume fluxes, are likely to be important in real lava channels.

The experiments were made possible by the enthusiastic technical assistance of Tony Beasley. We also thank Ross Wylde-Browne and Brad Ferguson for photographic assistance, and Graham Hughes for helpful comments. We acknowledge funding from ARC Discovery Grant DP0342569 and NSF Grant # EAR-9909507.

REFERENCES

Baker, V. R., Komatsu, G., Gulick, V. C. & Parker, T. J. 1997 Channels and valleys. In *Venus II* (ed. S. W. Bouger, D. M. Hunten & R. J. Phillips), pp. 757–798. University of Arizona Press.

Booth, B. & Self, S. 1973 Rheological features of the 1971 Mount Etna lavas. *Phil. Trans. R. Soc. Lond.* A **274**, 99–106.

Calvari, S., Coltelli, M., Neri, M., Pompilio, M. & Scribano, V. 1994 The 1991–93 Etna eruption: chronology and geological observations. *Acta Vulcanol.* **4**, 1–15.

Calvari, S. & Pinkerton, H. 1998 Formation of lava tubes and extensive flow field during the 1991–93 eruption of Mount Etna. *J. Geophys. Res.* **103**, 27291–27301.

Cashman, K. V., Pinkerton, H. & Stephenson, P. J. 1998 Long lava flows. *J. Geophys. Res.* **103**, 27281–27289.

Cashman, K. V., Thornber, C. R. & Kauahikaua, J. P. 1999 Cooling and crystallization of lava in open channels, and the transition of pahoehoe lava to ‘a‘a. *Bull. Volcanol.* **61**, 306–323.

Clever, R. M. & Busse, F. H. 1992 Three-dimensional convection in a horizontal fluid layer subjected to a constant shear. *J. Fluid Mech.* **234**, 511–527.

Crisp, J. & Baloga, S. 1990 A model for lava flows with two thermal components. *J. Geophys. Res.* **95**, 1255–1270.

Crisp, J. & Baloga, S. 1994 Influence of crystallisation and entrainment of cooler material on the emplacement of basaltic aa lava flows. *J. Geophys. Res.* **95**, 1255–1270.

Denton, R. A. & Wood, I. R. 1979 Turbulent convection between two horizontal plates. *Intl J. Heat Mass Transfer* **22**, 1339–1346.

Domaradzki, J. A. & Metcalfe, R.W. 1988 Direct numerical simulations of the effects of shear on turbulent Rayleigh-Bénard convection. *J. Fluid Mech.* **193**, 499–534.

Fink, J. H. & Griffiths, R. W. 1990 Radial spreading of viscous-gravity currents with solidifying crust. *J. Fluid. Mech.* **221**, 485–510.

Fink, J. H. & Griffiths, R. W. 1992 A laboratory analog study of the morphology of lava flows extruded from point and line sources. *J. Volcanol. Geotherm. Res.* **54**, 19–32.

Greeley, R. 1987 The role of lava tubes in Hawaiian volcanoes. *US Geol. Surv. Prof. Pap.* **1350**, 1589–1602.

Gregg, T. K. P. & Fink, J. H. 2000 A laboratory investigation into the effects of slope on lava flow morphology. *J. Volcanol. Geothermal Res.* **96**, 145–159.

Griffiths, R. W. 2000 The dynamics of lava flows. *Annu. Rev. Fluid Mech.* **32**, 477–518.

Griffiths, R. W. & Fink, J. H. 1992*a* The morphology of lava flows under planetary environments: predictions from analog experiments. *J. Geophys. Res.* **97**, 19,739–19,748.

Griffiths, R. W. & Fink, J. H. 1992*b* Solidification and morphology of submarine lavas: a dependence on extrusion rate. *J. Geophys. Res.* **97**, 19729–19737.

Griffiths, R. W. & Fink, J. H. 1993 Effects of surface cooling on the spreading of lava flows and domes. *J. Fluid Mech.* **252**, 667–702.

Griffiths, R. W. & Fink, J. H. 1997 Solidifying Bingham extrusions: a model for the growth of silicic lava domes. *J. Fluid Mech.* **347**, 13–36.

Guest, J. E., Underwood, J. R. & Greeley, R. 1980 The role of lava tubes in flows from Observatory Vent, 1971 eruption at Mount Etna, Sicily. *Bull. Volcanol.* **47**, 635–648.

Guest, J. E., Wood, C. & Greeley, R. 1984 Lava tubes, terraces and megatumuli on the 1614–24 pahoehoe lava flow field, Mount Etna. *Geol. Mag.* **117**, 601–606.

Hallworth, M. A., Huppert, H. E. & Sparks, R. S. J. 1987 A laboratory simulation of basaltic lava flows. *Mod. Geol.* **11**, 93–107.

Harris, A. J. L. & Rowland, S. K. 2001 FLOWGO: a kinematic thermo-rheological model for lava flowing in a channel. *Bull. Volcanol.* **63**, 20–44.

Hart, J. E. 1971 Stability of the flow in a differentially heated inclined box. *J. Fluid Mech.* **47**, 547–576.

Hon, K., Kauahikaua, J. P., Denlinger, R. & Mackay, K. 1994 Emplacement and inflation of pahoehoe sheets: observations and measurements of active lava flows on Kilauea Volcano, Hawai'I. *Geol. Soc. Am. Bull.* **106**, 351–370.

Hulme, G. 1974 The interpretation of lava flow morphology. *Geophys. J. R. Astron. Soc.* **39**, 361–383.

Ingersoll, A. P. 1966*a* Convective instabilities in plane Couette flow. *Phys. Fluids* **9**, 682–689.

Ingersoll, A. P. 1966*b* Thermal convection with shear at high Rayleigh numbers. *J. Fluid Mech.* **25**, 209–228.

Kauahikaua, J. P., Cashman, K. V., Mattox, T. N., Hon, K., Heliker, C. C., Mangan, M. T. & Thornber, C. R. 1998 Observations on basaltic lava streams in tubes from Kilauea Volcano, Hawai'i. *J. Geophys. Res.* **103**, 27303–27324.

Kerr, R. C. 1994 Melting driven by vigorous compositional convection. *J. Fluid Mech.* **280**, 255–285.

Kerr, R. C. 2001 Thermal erosion by laminar lava flows, *J. Geophys. Res.* **106**, 26453–26465.

Keszthelyi, L. 1995 A preliminary thermal budget for lava tubes on the Earth and planets. *J. Geophys. Res.* **100**, 20,411–20,420.

Kilburn, C. R. J. 1993 Lava crust, aa flow lengthening and the pahoehoe-aa transition. In *Active Lavas: Monitoring and Modelling* (ed. C. R. J. Kilburn & G. Luongo), pp. 263–279. UCL Press, London.

Lipman, P. W. & Banks, N. G. 1987 Aa flow dynamics, Mauna Loa 1984. *US Geol. Surv. Prof. Pap.* **1350**, 1527–1567.

Mouginis-Mark, P. J., Wilson, L. & Zuber, M. T. 1992 The physical volcanology of Mars. In *Mars* (ed. H. H. Keiffer, B. M. Jakosky, C. W. Snyder & M. S. Matthews), pp. 424–452. University of Arizona Press, Tucson.

Neal, C. A., Duggan, T. J., Wolfe, E. W. & Brand, E. L. 1988 Lava samples, temperatures, and compositions. *US Geol. Surv. Prof. Pap.* **1463**, 99–126.

Peterson, D. W., Holcomb, R. T., Tilling, R. I. & Christiansen, R. L. 1994 Development of lava tubes in the light of observations at Mauna Ulu, Kilauea Volcano, Hawaii. *Bull. Volcanol.* **56**, 343–360.

Pinkerton, H. & Wilson, L. 1994 Factors controlling the lengths of channel-fed lava flows. *Bull. Volcanol.* **56**, 108–120.

Richter, F. M. & Parsons, B. 1975 On the interaction of two scales of convection in the mantle. *J. Geophys. Res.* **80**, 2529–2541.

Ruddick, B. R. & Shirtcliffe, T. G. 1979 Data for double-diffusers: Physical properties of aqueous salt-sugar solutions. *Deep-Sea Res.* **26A**, 775–787.

Ryan, M. P. & Sammis, C. G. 1981 The glass transition in basalt. *J. Geophys. Res.* **86**, 9516–9539.

Sakimoto, S. E. H., Crisp, J., & Baloga, S. M. 1997 Eruption constraints on tube-fed planetary lava flows. *J. Geophys. Res.* **102**, 6597–6613.

Shaw, H. R. & Swanson, D. A. 1970 Eruption and flow rates of flood basalts. In *Proc. Second Columbia River Basalt Symposium* (ed. E. H. Gilmore & D. Stradling), pp. 271–299. Eastern Washington State College Press, Cheney.

Tallarico, A. & Dragoni, M. 1999 Viscous newtonian laminar flow in a rectangular channel: application to Etna lava flows. *Bull. Volcanol.* **61**, 40–47.

Tilling, R. I., Christiansen, R. L., Duffield, W. A., Endo, E.T., Holcomb, R. T., Koyanagi, R. Y., Peterson, D. W. & Unger, J. D., 1987 The 1972–1974 Mauna Ulu eruption, Kilauea Volcano: an example of quasi-steady-state magma transfer. *US Geol. Surv. Prof. Pap.* **1350**, 405–469.

Tolan, T. L., Reidel, S. P., Beeson, M. H., Anderson, J. L., Fecht, K. R. & Swanson, D. A. 1989 Revisions to the estimates of the areal extent and volume of the Columbia River Basalt Group. In *Volcanism and Tectonism in the Columbia River Flood-Basalt Province* (ed. S. P. Reidel & P. R. Hooper), *Geol. Soc. Amer. Spec. Pap.* **239**, 1–20.

Turner, J. S. 1973 *Buoyancy Effects in Fluids*. Cambridge University Press.

Walker, G. P. L. 1973 Factors controlling the lengths of lava flows. *Phil. Trans. R. Soc. Lond.* **274**, A 107–118.

Walton, I. C. 1985 The effect of a shear flow on convection in a layer heated non-uniformly from below. *J. Fluid Mech.* **154**, 303–319.

Washburn, E. W. (Ed.) 1926 *International Critical Tables of Numerical data: Physics, Chemistry and Technology*. National Academic press.

White, F. M. 1991 *Viscous Fluid Flow*, 2nd Edn., McGraw-Hill.

Wilson, L. & Head, J. W. 1983 A comparison of volcanic eruption processes on Earth, Moon, Mars, Io, and Venus. *Nature* **302**, 663–669.

Zimbelman, J. R. & Gregg, T. K. P. (Eds.) 2000 *Environmental Effects on Volcanic Eruptions: From Deep Oceans to Deep Space*. Kluwer/Plenum.